Spin- and isospin-polarized states of nuclear matter in the Dirac-Brueckner-Hartree-Fock model

Francesca Sammarruca*
Physics Department, University of Idaho, Moscow, Idaho 83844-0903, USA
(Received 11 April 2011; published 7 June 2011)

Spin-polarized isospin asymmetric nuclear matter is studied within the Dirac-Brueckner-Hartree-Fock approach. After a brief review of the formalism, we present and discuss the self-consistent single-particle potentials at various levels of spin and isospin asymmetry. We then move to predictions of the energy per particle, also under different conditions of isospin and spin polarization. Comparison with the energy per particle in isospin symmetric or asymmetric unpolarized nuclear matter shows no evidence for a phase transition to a spin-ordered state, neither ferromagnetic nor antiferromagnetic.

DOI: 10.1103/PhysRevC.83.064304 PACS number(s): 21.30.Fe, 21.65.Cd, 21.65.Mn, 21.60.Jz

I. INTRODUCTION

Describing the properties of nuclear matter, especially under extreme conditions, is a topic of current interest which still presents considerable theoretical challenges. Of particular interest is the equation of state of matter with unequal concentrations of protons and neutrons, because of its many applications ranging from the physics of rare isotopes to the properties of neutron stars. In spite of recent and fast-growing effort, the density dependence of the symmetry energy is not sufficiently constrained and theoretical predictions show considerable model dependence.

When isospin and spin asymmetries are considered together, available constraints are even more limited and predictions regarding magnetic properties of nuclear matter are sometimes found to be in qualitative disagreement. Polarization properties of neutron and nuclear matter have been studied extensively with a variety of theoretical methods [1–28], often with contradictory conclusions. In the study in Ref. [29], the possibility of phase transitions into spin-ordered states of symmetric nuclear matter was explored based on the Gogny interaction [30] and the Fermi liquid formalism. There, the appearance of an antiferromagnetic state (with opposite spins for neutrons and protons) was predicted, whereas the transition to a ferromagnetic state was not observed. This is in contrast with predictions based on the Skyrme interaction [31].

The properties of polarized neutron matter (NM), in particular, have gathered much attention lately, in conjunction with the issue of ferromagnetic instabilities together with the possibility of strong magnetic fields in the interior of rotating neutron stars. The presence of polarization would impact neutrino cross section and luminosity, resulting in a very different scenario for neutron star cooling.

There are other, equally important, motivations to undertake studies of polarized matter. In Ref. [32], for instance, we focused on the spin degrees of freedom of symmetric nuclear matter (SNM), having in mind a terrestrial scenario as a possible "laboratory." We payed particular attention to the spin-dependent *symmetry potential*, namely the gradient between the single-nucleon potentials for upward and downward polarized nucleons in SNM. The interest around this quantity arises because of its natural interpretation as a spin-dependent nuclear optical potential, defined in perfect formal analogy to the Lane potential [34] for the isospin degree of freedom in isospin-asymmetric nuclear matter (IANM).

Whether one is interested in rapidly rotating pulsars or more conventional nuclear physics, it is important to consider the general case where both spin and isospin asymmetries can be present. First, neutron star matter contains a nonnegligible proton fraction. Concerning laboratory nuclear physics, one way to access information related to the spin dependence of the nuclear interaction in nuclear matter is the study of collective modes such as giant resonances. Because a spin unsaturated system is usually also isospin asymmetric, both degrees of freedom need to be taken into account.

In previous calculations [32,33], we have investigated spin-polarized pure neutron matter and symmetric matter. The purpose of this paper is to extend our previous predictions to include matter with different concentrations of neutrons and protons where each nucleon species can have definite spin polarization. Our framework consists of the Dirac-Brueckner-Hartree-Fock (DBHF) approach to nuclear matter together with a realistic meson-theoretic potential, which we choose to be the Bonn B potential [35]. To the best of our knowledge, this kind of calculation for spin-polarized asymmetric nuclear matter (SPANM) is not in the literature.

This paper is organized as follows. In the next section we review the main aspects of the procedure leading to the self-consistent determination of the one-body potentials experienced by a single nucleon in SPANM together with the effective interaction. The characteristics of those potentials are discussed in Sec. III. We then proceed to show results for the energy per particle, namely the equation of state (EoS) of SPANM under extreme conditions of polarization (Sec. IV). The existence (or not) of a possible phase transition can be argued by comparing the energies of the fully polarized and the unpolarized phases. A brief summary and our conclusions are contained in the last section.

II. BRIEF REVIEW OF THE SELF-CONSISTENT METHOD

Our calculation is microscopic and treats nucleons relativistically. Within the Dirac-Brueckner-Hartree-Fock (DBHF) method, the interactions of the nucleons with the

*fsammarr@uidaho.edu

nuclear medium are expressed as self-energy corrections to the nucleon propagator. That is, the nucleons are regarded as "dressed" quasiparticles. Relativistic effects lead to an intrinsically density-dependent interaction which is approximately consistent with the contribution from three-body forces (TBF) typically employed in nonrelativistic approaches, particularly those TBF of the "Z-diagram" type, which originate from the presence of negative energy Dirac states (antinucleons).

The starting point of any microscopic calculation of nuclear structure or reactions is a realistic free-space nucleon-nucleon interaction. Our standard framework consists of the Bonn B one-boson-exchange (OBE) potential [35] together with the DBHF approach to nuclear matter. A detailed description of our application of the DBHF method to SNM, NM, and IANM can be found in a recent review of our work [36]. (In the bibliography of Ref. [36] the reader will find a fairly complete list of original DBHF papers concerning SNM.)

In a spin-polarized and isospin asymmetric system with fixed total density ρ, the partial densities of each species are

$$\rho_n = \rho_{nu} + \rho_{nd}, \quad \rho_p = \rho_{pu} + \rho_{pd}, \quad \rho = \rho_n + \rho_p, \tag{1}$$

where u and d refer to up and down spin polarizations, respectively, of protons (p) or neutrons (n). The isospin and spin asymmetries, α, β_n, and β_p, are defined in a natural way:

$$\alpha = \frac{\rho_n - \rho_p}{\rho}, \quad \beta_n = \frac{\rho_{nu} - \rho_{nd}}{\rho_n}, \quad \beta_p = \frac{\rho_{pu} - \rho_{pd}}{\rho_p}. \tag{2}$$

The density of each individual component can be related to the total density by

$$\rho_{nu} = \frac{1+\beta_n}{2}\frac{1+\alpha}{2}\rho, \tag{3}$$

$$\rho_{nd} = \frac{1-\beta_n}{2}\frac{1+\alpha}{2}\rho, \tag{4}$$

$$\rho_{pu} = \frac{1+\beta_p}{2}\frac{1-\alpha}{2}\rho, \tag{5}$$

$$\rho_{pd} = \frac{1-\beta_p}{2}\frac{1-\alpha}{2}\rho, \tag{6}$$

where each partial density is related to the corresponding Fermi momentum through $\rho_{\tau\sigma} = \frac{(k_F^{\tau\sigma})^3}{6\pi^2}$. The *average* Fermi momentum and the total density are related in the usual way as $\rho = \frac{2k_F^3}{3\pi^2}$.

The single-particle potential of a nucleon in a particular $\tau\sigma$ state, $U_{\tau\sigma}$, is the solution of a set of four coupled equations,

$$U_{nu} = U_{nu,nu} + U_{nu,nd} + U_{nu,pu} + U_{nu,pd}, \tag{7}$$

$$U_{nd} = U_{nd,nu} + U_{nd,nd} + U_{nd,pu} + U_{nd,pd}, \tag{8}$$

$$U_{pu} = U_{pu,nu} + U_{pu,nd} + U_{pu,pu} + U_{pu,pd}, \tag{9}$$

$$U_{pd} = U_{pd,nu} + U_{pd,nd} + U_{pd,pu} + U_{pd,pd}, \tag{10}$$

to be solved self-consistently along with the two-nucleon G matrix. In the above equations, each $U_{\tau\sigma,\tau'\sigma'}$ term contains the appropriate (spin and isospin dependent) part of the interaction, $G_{\tau\sigma,'\tau'\sigma'}$. More specifically,

$$U_{\tau\sigma}(\vec{k}) = \sum_{\sigma'=u,d}\sum_{\tau'=n,p}\sum_{q\leqslant k_F^{\tau'\sigma'}} \langle \tau\sigma, \tau'\sigma' | G(\vec{k},\vec{q}) | \tau\sigma, \tau'\sigma' \rangle, \tag{11}$$

where the third summation indicates integration over the Fermi seas of protons and neutrons with spin-up and spin-down, and

$$\begin{aligned}
&\langle \tau\sigma, \tau'\sigma' | G(\vec{k},\vec{q}) | \sigma\tau, \sigma'\tau' \rangle \\
&= \sum_{L,L',S,J,M,M_L,T} \left| \left\langle \frac{1}{2}\sigma; \frac{1}{2}\sigma' | S(\sigma+\sigma') \right\rangle \right|^2 \\
&\quad \times \left| \left\langle \frac{1}{2}\tau; \frac{1}{2}\tau' | T(\tau+\tau') \right\rangle \right|^2 \langle L M_L; S(\sigma+\sigma') | J M \rangle \\
&\quad \times \langle L' M_L; S(\sigma+\sigma') | J M \rangle i^{L'-L} Y^*_{L',M_L}(\hat{k}_{rel}) Y_{L,M_L}(\hat{k}_{rel}) \\
&\quad \times \langle L S J | G(k_{rel}, K_{cm}) | L' S J \rangle.
\end{aligned} \tag{12}$$

Consistent with the DBHF method, the G matrix contains medium effects from Pauli blocking, dispersion, and modification of the spin-dependent nucleon field applied to the nucleon-nucleon potential.

The need to separate the interaction by spin components brings along angular dependence, with the result that the single-particle potential depends also on the direction of the momentum, although such dependence was found to be weak [33]. The G-matrix equation is solved using partial wave decomposition and the matrix elements are then summed as in Eq. (12) to provide the new matrix elements in the representation needed for Eq. (11), namely with spin and isospin components explicitly projected out. Furthermore, the scattering equation is solved using relative and center-of-mass coordinates, k_{rel} and K_{cm}, since the former is a natural coordinate for the evaluation of the nuclear potential. Those are then easily related to the momenta of the two particles, k and q, in order to perform the integration indicated in Eq. (11). Notice that solving the G-matrix equation requires knowledge of the single-particle potential, which in turn requires knowledge of the effective interaction. Hence, Eqs. (7)–(10) together with the G-matrix equation constitute a rather lengthy self-consistency problem. The latter starts with an ansatz for the single-particle potential as suggested by the most general structure of the nucleon self-energy operator consistent with all symmetry requirements. (See Ref. [36] and references therein.) Parametrization of the ansatz and comparison with Eq. (11) at every step of the iterative procedure, a method known as the "reference spectrum approximation," allow the determination of the single-nucleon potentials in each $\tau\sigma$ channel.

The kernel of the G-matrix equation contains the Pauli operator for scattering of two particles with two different Fermi momenta, $k_F^{\tau\sigma}$ and $k_F^{\tau'\sigma'}$, which is defined in analogy with the one for IANM [37],

$$Q_{\tau\sigma,\tau'\sigma'}\left(k, q, k_F^{\tau\sigma}, k_F^{'\tau'\sigma'}\right) = \begin{cases} 1 & \text{if } p > k_F^{\tau\sigma} \text{ and } q > k_F^{\tau'\sigma'}, \\ 0 & \text{otherwise.} \end{cases} \tag{13}$$

The Pauli operator is then expressed in terms of $k_{\rm rel}$ and $K_{\rm cm}$ and angle averaged in the usual way.

Once a self-consistent solution for Eqs. (7)–(11) has been obtained, the average potential energy for a given $\tau\sigma$ component can be calculated. A final average over all $\tau\sigma$ components provides, along with the kinetic energy $K_{\tau\sigma}$, the average energy/particle in spin-polarized isospin-asymmetric

nuclear matter. Specifically,

$$\frac{E}{A} = \frac{1}{A} \sum_{\sigma=u,d} \sum_{\tau=n,p} \sum_{k \leqslant k_F^{\tau\sigma}} \left(K_{\tau\sigma}(k) + \frac{1}{2} U_{\tau\sigma}(k) \right), \quad (14)$$

where E/A is a function of ρ, α, β_n, and β_p. We recall that, in the DBHF approach, the kinetic energy is obtained from the expectation value of the free-particle operator in the Dirac equation.

All calculations are conducted including values of the total angular momentum from 0 to 6, which we have verified to provide satisfactory convergence.

III. ONE-BODY POTENTIALS IN SPANM

The single-particle potential in nuclear matter is a very important quantity as it can be viewed as the optical potential in the interior of a nucleus and thus, to a certain extent, can be constrained by optical potential analyses. In this section, we present and discuss its dependence on the momentum and on spin/isospin asymmetries.

A. Momentum dependence

In Fig. 1(a) we show the momentum dependence of the one-body potentials for upward- and downward-polarized neutrons in isospin symmetric ($\alpha = 0$) nuclear matter. The protons are unpolarized whereas the neutron spin polarization parameter is taken to be 0.6. Figure 1(b) shows the same quantity for protons. In both cases, the solid curve is the prediction of the single-particle potential in unpolarized matter. All potentials are calculated at a density equal to 0.185 fm^{-3}. In all cases, the polar angle of the momentum vector $\vec{k}$ is taken to be zero.

With a larger number of upward-polarized neutrons, $U_{nu}(k)$ becomes more repulsive while $U_{nd}(k)$ turns more attractive. Notice that the opposite trend is displayed by $U_{pu}(k)$ and $U_{pd}(k)$. The reason for the observed splittings is of course in the spin dependence of the G matrix (and isospin dependence, when applicable), together with the fact that the number of interactions a single nucleon (with specified $\tau\sigma$) can undergo with other ($\tau'\sigma'$) nucleons changes as the population of one species increases or decreases.

Figures 1(c)–1(d) show a situation parallel to the one presented in Figs. 1(a)–1(b), except that the neutrons are now unpolarized. Comparison between Figs. 1(a)–1(b) and Figs. 1(c)–1(d) shows that, as can be expected, the roles of neutrons and protons are perfectly interchanged when $\beta_n \to \beta_p$ and $\beta_p \to \beta_n$.

In Figs. 1(e)–1(f), we investigate the impact of including isospin asymmetry as well, specifically a neutron excess given by $\alpha = 0.5$. [Notice that the neutron and proton potentials in absence of polarization (solid curves) are different to begin with due to the isospin asymmetry.] The splitting remains qualitatively similar to the case seen in Figs. 1(a)–1(b), but it is more pronounced for the nucleon type whose density is larger.

In all cases, the momentum dependence remains qualitatively similar to the one displayed in unpolarized SNM, with the size of the splitting larger at the lower momenta, which may be due to weaker sensitivity of a high-momentum nucleon to medium and asymmetry effects.

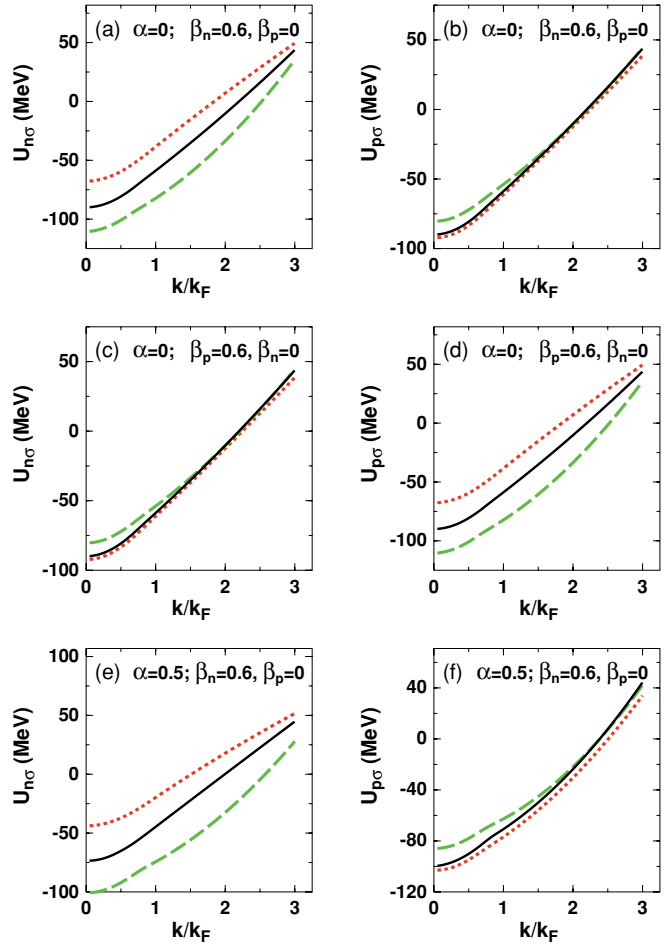

FIG. 1. (Color online) The neutron (left side) and the proton (right side) single-particle potentials in isospin symmetric or asymmetric matter with isospin asymmetry and neutron and proton polarizations as indicated inside the frames. The (black) solid line is the prediction for unpolarized matter. In all frames, the (red) dotted and (green) dashed lines are the predicted $U_{\tau u}$ and $U_{\tau d}$, respectively. The horizontal axis is the momentum in units of the average Fermi momentum, which is equal to 1.4 fm^{-1}.

B. Spin and isospin asymmetry dependence

Here we focus on the dependence of the single-particle potentials on various levels of asymmetries, for fixed total density and momentum $\vec{k}$. First, we show the splitting of the single-neutron and single-proton potentials in isospin symmetric matter with changing neutron polarization (and for zero proton polarization), see Fig. 2(a). Figure 2(b) confirms that the appropriate symmetry is respected when neutron and proton polarizations are interchanged.

For the predictions of Figs. 2(c)–2(d), isospin asymmetry has been introduced as well. Notice that the predictions shown in Figs. 2(c)–2(d) are not, and should not be, symmetric with respect to $n \leftrightarrow p$ exchange. This is the case if $\alpha \to -\alpha$,

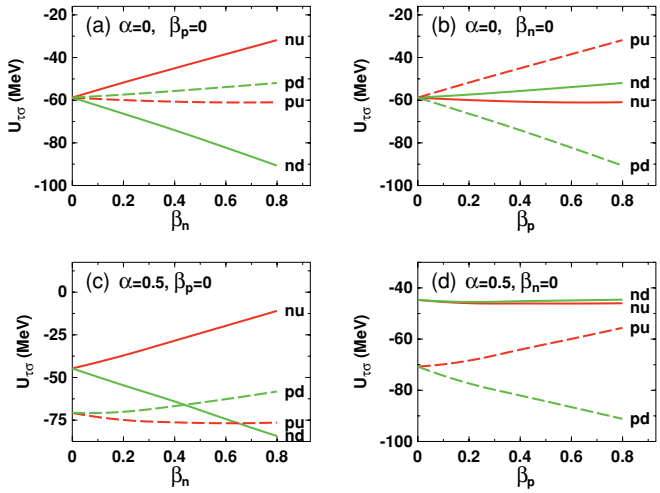

FIG. 2. (Color online) The neutron (solid lines) and the proton (dashed lines) single-particle potentials in isospin symmetric or asymmetric matter vs the neutron (left side) and the proton (right side) spin polarizations. The nucleon momentum is fixed and equal to the average Fermi momentum, 1.4 fm^{-1}.

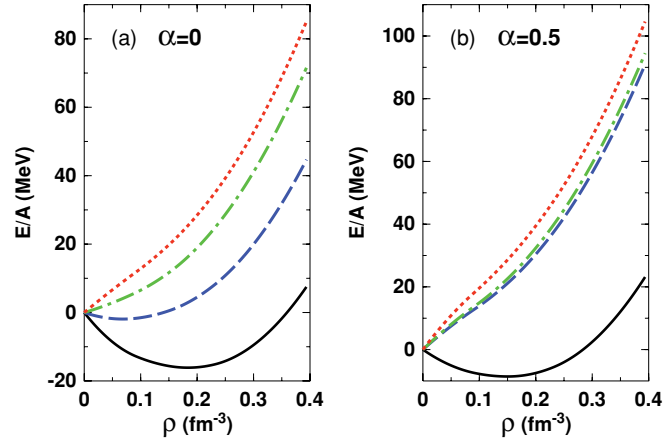

FIG. 3. (Color online) The energy per particle as a function of density and various degrees of proton and neutron polarizations in symmetric matter (left) and asymmetric matter (right). In both frames, the (blue) dashed line corresponds to totally polarized neutrons and unpolarized protons ($\beta_n = 1, \beta_p = 0$); the (green) dash-dotted line is the prediction for the FM state ($\beta_n = 1, \beta_p = 1$); the (red) dotted line shows the energy of the AFM state ($\beta_n = 1, \beta_p = -1$). The (black) solid line shows the predictions for unpolarized matter.

in addition to $\beta_n \to \beta_p$ and $\beta_p \to \beta_n$ (that is, under charge exchange).

As pointed out in the previous subsection, the size and direction of the various splittings depend sensitively on the strength of the partial contributions, $U_{\tau\sigma,\tau'\sigma'}$, to each $U_{\tau\sigma}$ potential, see Eqs. (7)–(11), which in turn receive contributions from G-matrix elements in different spin and isospin channels. We will come back to this point in the next section when discussing the energy per particle.

The curves displayed in Figs. 2(a)–2(d) show an approximately linear behavior, although some deviations from linearity can be seen, especially for the weaker potentials in asymmetric matter. We observed a similar trend when only isospin splitting or only spin splitting (in NM or SNM) was considered [32].

IV. ENERGY PER PARTICLE IN SPANM

When the potential and kinetic energies are averaged as in Eq. (14), one obtains the energy per nucleon for a given state of isospin asymmetry and spin polarization. To render the four-dimensional self-consistent calculation more manageable, we ignore the angular dependence, which was found to be weak both in nuclear and in neutron matter [16,33], and keep the polar angle of the nucleon momentum vector at a constant value, for which we choose $\pi/4$. We have tested this choice in a few cases and found it to give good agreement with the result of averaging over all angles. (Notice that single-nucleon potentials in polarized matter have their maximum or minimum values at either zero or $\pi/2$.)

In the left panel of Fig. 3, we show, in comparison with unpolarized symmetric matter (solid line), the EoS for the case of fully polarized neutrons and completely unpolarized protons (dashed line); the EoS for the case of protons and neutrons totally polarized in the same direction, that is, matter in the ferromagnetic (FM) state (dashed-dotted line); and the EoS for the case of protons and neutrons totally polarized in opposite directions, namely, matter in the antiferromagnetic (AFM) state (dotted line). A similar comparison is shown in the right panel of Fig. 3, but for isospin asymmetric matter. (Notice that all predictions are invariant under a global spin flip, as we have verified directly.)

To better understand our findings, we have examined the contributions to the potential energy from singlet and triplet states separately. Taking as an example the case of unpolarized asymmetric matter, up to the densities considered here (about 0.4 fm^{-3}) the contribution to the potential energy from singlet states was found to be attractive. Such contribution is absent in the fully polarized case, implying increased repulsion in the latter. Concerning triplet states, we found their contribution to the potential energy to be more repulsive in the fully polarized case as compared to the unpolarized one. A similar analysis can explain the origin of the larger energy in the AFM state as compared to the unpolarized one.

In summary, we find that, for both symmetric and asymmetric matter, the energies of the FM and AFM states are higher than those of the corresponding unpolarized cases, with the AFM state being the most energetic. Thus, a phase transition is not anticipated in our model. This conclusion seems to be shared by predictions of microscopic models, such as those based on conventional Brueckner-Hartree-Fock theory [18]. On the other hand, calculations based on various parametrizations of Skyrme forces result in different conclusions. For instance, with the SLy4 and SLy5 forces and the Fermi liquid formalism a phase transition to the AFM state is predicted in asymmetric matter at a critical density equal to about 2–3 times the normal density [29].

It is interesting to observe that models based on realistic nucleon-nucleon potentials, whether relativistic or nonrelativistic, are at least in qualitative agreement with one

another in predicting more energy for totally polarized states (FM or AFM) up to densities well above normal density. For instance, our predictions are in good agreement with the corresponding ones from Ref. [18]. In particular, the qualitative behavior of the various curves relative to one another is remarkably consistent, considering differences in the many-body approaches (BHF vs DBHF) and the bare two-nucleon interactions (Bonn B vs model NSC97e by the Nijmegen group [38]). The main signature of the DBHF framework is additional repulsion due to the quenching of the σ contribution in the medium associated with the reduction of the nucleon mass. This is especially noticeable at densities above saturation, where the relativistic Dirac effect becomes stronger. Indeed, quantitatively speaking, our energies do show more repulsion. On the other hand, the Nijmegen model for the nucleon-nucleon interaction is more repulsive than Bonn B (without Dirac effect) due to a stronger tensor force (typical for a local potential). The combination of these two mechanisms, and their relative importance as a function of density, is most likely the reason why the agreement between our predictions and those from Ref. [18] may be better than expected.

On the other hand, *qualitative* disagreement is encountered with nonmicroscopic approaches [29] and also with relativistic Hartree-Fock models based on effective nucleon-meson Lagrangians. For instance, in Ref. [12] it was reported that the onset of a ferromagnetic transition in neutron matter, and its critical density, are crucially determined by the inclusion of isovector mesons and the nature of their couplings. Notice that our microscopic model also includes the isovector mesons π, ρ, and δ (a_0), but does not predict a similar scenario. The reason for this difference is most likely due to the fact that in our model all meson-nucleon couplings are constrained by a fit to the free-space nucleon-nucleon data. In relativistic Hartree-Fock models no such constraints are applied.

V. CONCLUSIONS

Continuing with our broad analysis of nuclear matter and its extreme states, we have extended our framework and gone beyond existing predictions. As usual, we adopt the microscopic approach for our nuclear matter calculations. Concerning our many-body method, we find DBHF to be a good starting point to look beyond the normal states of nuclear matter, which it describes successfully. The main strength of this method is its inherent ability to effectively incorporate crucial TBF contributions through relativistic effects.

In this paper, we extended previous calculations to incorporate the general case of spin and isospin unsaturated matter. Our main result is that we do not predict, or foresee, a phase transition to a ferromagnetic or antiferromagnetic state. In microscopic models one starts with the bare interaction and includes correlations through the G-matrix calculation, where all important meson contributions are constrained by free-space data. The handling of spin and isospin dependent amplitudes, in particular, whether they are tightly constrained or not, is most likely at the origin of the divergence of predictions between microscopic and nonmicroscopic approaches.

In the near future, we hope to construct a convenient and sufficiently accurate parametrization of our ρ, α, β_n, and β_p dependent EoS. This may be helpful for application purposes, given that the self-consistency problem can be time consuming.

We point out that empirical constraints are desirable to test predictions of the spin and isospin dependence of nuclear matter properties. At normal densities, systematic analyses of spin- and isospin-dependent optical potentials can help constrain $U_{\sigma\tau}$.

ACKNOWLEDGMENTS

Support from the US Department of Energy under Grant No. DE-FG02-03ER41270 is acknowledged.

[1] D. H. Brownell and J. Callaway, Nuovo Cimento B **60**, 169 (1969).
[2] M. J. Rice, Phys. Lett. A **29**, 637 (1969).
[3] J. W. Clark and N. C. Chao, Lett. Nuovo Cimento **2**, 185 (1969).
[4] J. W. Clark, Phys. Rev. Lett. **23**, 1463 (1969).
[5] S. D. Silverstein, Phys. Rev. Lett. **23**, 139 (1969).
[6] E. Østgaard, Nucl. Phys. A **154**, 202 (1970).
[7] J. M. Pearson and G. Saunier, Phys. Rev. Lett. **24**, 325 (1970).
[8] V. R. Pandharipande, V. K. Garde, and J. K. Srivastava, Phys. Lett. B **38**, 485 (1972).
[9] S. O. Bäckmann and C. G. Källman, Phys. Lett. B **43**, 263 (1973).
[10] P. Haensel, Phys. Rev. C **11**, 1822 (1975).
[11] J. Dabrowski, Can. J. Phys. **62**, 400 (1984).
[12] S. Marcos, R. Niembro, M. L. Quelle, and J. Navarro, Phys. Lett. B **271**, 277 (1991).
[13] M. Kutshera and W. Wojcik, Phys. Lett. B **223**, 11 (1989).
[14] P. Bernardos, S. Marcos, R. Niembro, and M. L. Quelle, Phys. Lett. B **356**, 175 (1995).
[15] S. Fantoni, A. Sarsa, and K. E. Schmidt, Phys. Lett. **87**, 181101 (2001).
[16] T. Frick, H. Müther, and A. Sedrakian, Phys. Rev. C **65**, 061303 (2002).
[17] I. Vidaña, A. Polls, and A. Ramos, Phys. Rev. C **65**, 035804 (2002).
[18] I. Vidaña and Ignazio Bombaci, Phys. Rev. C **66**, 045801 (2002).
[19] A. A. Isayev and J. Yang, Phys. Rev. C **69**, 025801 (2004).
[20] Fabio L. Braghin, Phys. Rev. C **71**, 064303 (2005).
[21] N. Kaiser, Phys. Rev. C **70**, 054001 (2004).
[22] A. Rios, A. Polls, and I. Vidaña, Phys. Rev. C **71**, 055802 (2005).
[23] M. Kutshera and W. Wojcik, Phys. Lett. B **325**, 271 (1994).
[24] A. Vidaurre, J. Navarro, and J. Bernabéu, Astron. Astrophys. **135**, 361 (1984).
[25] I. Bombaci, A. Polls, A. Ramos, A. Rios, and I. Vidaña, Phys. Lett. B **632**, 638 (2006).

[26] V. S. Uma Maheswari, D. N. Basu, J. N. De, and S. K. Samaddar, Nucl. Phys. A **615**, 516 (1997).
[27] W. Zuo, U. Lombardo, and C. W. Shen, in *Quark-Gluon Plasma and Heavy Ion Collisions*, edited by W. M. Alberico *et al.* (World Scientific, Singapore, 2002), p. 192.
[28] W. Zuo, Caiwan Shen, and U. Lombardo, Phys. Rev. C **67**, 037301 (2003).
[29] A. A. Isayev and J. Yang, Phys. Rev. C **70**, 064310 (2004).
[30] J. Decharge and D. Gogny, Phys. Rev. C **21**, 1568 (1980).
[31] A. A. Isayev, JETP Lett. **77**, 251 (2003).
[32] F. Sammarruca, Phys. Rev. C **82**, 027307 (2010).
[33] F. Sammarruca and P. G. Krastev, Phys. Rev. C **75**, 034315 (2007).
[34] A. M. Lane, Nucl. Phys. **35**, 676 (1962).
[35] R. Machleidt, Adv. Nucl. Phys. **19**, 189 (1989).
[36] F. Sammarruca, Int. J. Mod. Phys. E **19**, 1259 (2010).
[37] D. Alonso and F. Sammarruca, Phys. Rev. C **67**, 054301 (2003).
[38] V. G. J. Stoks and Th. A. Rijken, Phys. Rev. C **59**, 3009 (1999).